International Journal of Fluid Power 6 (2005) No. 3 pp. 5-18

MODEL AND EXPERIMENTAL VALIDATION OF A LOAD SENSING SYSTEM WITH A CRITICALLY LAPPED REGULATOR SPOOL

Duqiang Wu [1], Greg Schoenau [2], Richard Burton [2] and Doug Bitner [2]

[1] Lead Engineer, Eaton Corp, Minneapolis
[2] Department of Mechanical Engineering, University of Saskatchewan
57 Campus Drive, Saskatoon, Saskatchewan, Canada, S7N 5A9
duqiangwu@eaton.com

Abstract

A load sensing (LS) system is one in which the pump flow is regulated to keep the pressure drop across an orifice constant and independent of any variation in the load pressure. This ensures that the pressure loss across the orifice is kept to a minimum, thereby increasing efficiency. An LS regulator spool is used to sense the pressure drop across the orifice to control pump delivery. The spool can be underlapped, critically lapped or overlapped. As a trade-off between efficiency and dynamic response, the LS spool is usually critically lapped. This results in a nonlinear model that is sensitive to operating regions.

In this paper, a review of published literature on LS systems is briefly summarized. An LS system model is developed and linearized. Procedures to solve these very complex equations are introduced. Because load sensing systems require pressure feedback, stability can often be an issue. Analysis of these systems to determine the steady state and dynamic performance is very difficult to do because of the dependency of the models on the operating point. Linearized models which reflect a methodology to account for changing operating conditions have been developed and have established three distinct regions of operation (labeled "Conditions I, II, and III"). This paper presents the experimental nature of these conditions and provides experimental evidence that the models so derived are valid over certain frequency ranges. The objective of this paper, then, was to establish confidence in the models by examining frequency response performance under these three distinct conditions. The results show that good agreement does exist between the models and their physical counterparts and establishes limitations thereof.

This research can assist in the design or optimization of an LS system and help in the development of advanced control strategies for obtaining further efficiency within certain dynamic performance constraints.

Keywords: load sensing, stability, linearization, operating point, energy efficiency

1 Introduction

A load sensing (LS) system is one in which the pump flow is regulated to keep the pressure drop across an orifice constant independent of the load pressure. This regulation process is achieved by feeding back the pressure drop across the orifice to a control valve (usually denoted as a LS regulator) at the LS pump. This ensures that the pressure loss across the orifice is kept to a minimum. In order to reduce the energy loss on the LS regulator and to further improve the overall efficiency of the LS system, the LS regulator is usually designed with a critically lapped spool. However, stability problems and undesirable interactions amongst loads have been reported (Lantto et al, 1990 and Lantto et al, 1991).

Considerable research has been conducted into understanding and compensating for stability problems. Bitner and Burton, (1984(1)) and Bitner (1984(2)) addressed the measurement technique of load sensing pump parameters for a LS system. This research indicated that two factors, fluid temperature and the system operating point, greatly affected the flow gain and flow-pressure coefficient of the orifice, the leakage of the pump, and the frequency response. Palmberg et al (1985) provided a model of a pressure-control pump that is used in most LS simulations. It was found that the dynamic performance of the pressure-control pump was mainly influenced by the pump inductance, and to

This manuscript was received on 2 November 2004 and was accepted after revision for publication on 3 September 2005

a lesser degree, by the break frequency and leakage coefficient of the pump.

Kim et al (1988) developed linearized frequency domain models that included a stability analysis using the Routh-Hurwitz criterion. The model did not consider the damping of the load sensing line and the LS pump was only considered as a simple 2nd order system. Krus (1988) provided a detailed model of a LS system. A general transfer function was presented, composed of three subsystems (the pump and pump regulator, valve systems, and loads). A stability criterion was established for a simple inertia load. Two main instabilities (pump high-frequency instability for small valve openings and pump-load low-frequency at large valve openings) were described qualitatively. In addition, two other instabilities (load low-frequency instability at small valve openings and pump-load high-frequency instability at large valve openings) were also mentioned.

In the study by Lantto et al (1991) and indeed others (Bitner, 1986; Kim and Cho, 1988), the complete LS system has been observed to enter into limit cycle conditions (a stability problem). Sakurai and Takahashi (1997) used a bond-graph model of the LS system to investigate overall efficiency taking into consideration the dynamic characteristics of the system. It was found that there was a point of maximum overall efficiency. Simulations by Book and Goering (1997) verified that instabilities caused by the inertia load could be eliminated with the addition of damping in the feedback line.

Erkkila (1999) provided a block diagram of an LS system to assist in the dynamic analysis of LS systems. An analogue-mechanical model and an analogue-electrical model for a LS system were also provided. Kappl (2001) used experimental methods to obtain a semi-empirical model for the variable displacement pump with a load sensing regulator and power restrictor. Zarotti and Nervegna (1988) addressed the "non-standard" operation of LS systems. Three-dimensional plots of output flow of a single load LS system showed the favorable operating range that would be expected.

A common objective of the aforementioned research using linearization was to generate an understanding of the relationship between the LS hydraulic circuit parameters (component structure parameters and adjustable parameters) and the dynamic response of LS systems leading to a design that demonstrated controllability and energy efficiency. For example, it is essential that the LS system be stable over the full range of the flow orifice opening. This is difficult to achieve due to non-linearities of LS systems.

Analysis using the various models' linearization operating point had limited effectiveness. The transfer function of LS systems and the stability criterion so developed include the flow gain and the flow-pressure coefficient that are strongly affected by the operating point. In reality, the main parameters used in the stability analysis (flow gain, K_q, and flow-pressure coefficient, K_c, of valves) were a function of state variables of the system, such as the spool displacement and system pressure. Thus, any stability criterion developed from transfer functions could only be considered meaningful if all the linearized parameters (K_c, K_q) had "reasonable" values.

Wu et al (2002(1)) identified three different steady state operating regions and their transition regions for a typical LS system with an LS regulator made up of a critically lapped spool, and presented a set of steady state models for solving the operating point locations in different operating regions. A precise model of the LS system was developed for these regions.

In order to develop a valid model (i.e. transfer function) to identify stability in each operating region, it is essential that the linearized parameters (flow gain K_{cr}, and flow-pressure coefficient K_{qr}) of the LS regulator be evaluated. The flow gain K_c and flow-pressure coefficient K_q of orifices are usually computed by the well-known flow equation Merritt (1967):

$$Q = C_d wx\sqrt{\frac{2}{\rho}(P_s - P_L)}$$

Because the leakage flow through the LS regulator is small, (due to a critically lapped spool), and hence laminar, the discharge coefficient C_d in the above equation becomes a function of the Reynolds number and hence a function of the flow rate, i.e.

$$Q = C_d(Q)wx\sqrt{\frac{2}{\rho}(P_s - P_L)}\cdot$$

Therefore, the traditional formulas

$$K_q = C_d w\sqrt{\frac{2}{\rho}(P_{s0} - P_{L0})}$$

and

$$K_c = \frac{C_d wx}{\sqrt{2\rho(P_{s0} - P_{L0})}}$$

are invalid for the LS regulator. Wu et al (2002(2)) developed an empirical model of the discharge coefficient $C_d(Q)$ which was used in the calculation of flow through the LS regulator. Wu et al (2003) further solved the discontinuity problem when applying the equation to the null position ($x = 0$).

The objective of this paper is to introduce a comprehensive nonlinear model of the LS system. Three different steady state operating conditions defined as "Conditions I, II and III" are discussed. A procedure for solving the many nonlinear equations is presented, and the governing equations are validated experimentally. Because of the number of equations that are required to complete the models, only the final transfer function forms are presented in this paper. Detailed derivations of the transfer functions can be found in Wu (2003).

2 LS System and Component Model

Figure 1 is a schematic of an LS system with a critically lapped spool in the LS regulator. The system consists of an axial piston pump with an LS regulator and a control piston, an adjustable flow orifice, an LS line with a damping orifice and a motor with a load attached. The system operation is governed by three dy-

namic displacement equations associated with the displacement of the LS spool, x_r, the swash plate angle, θ_{sp}, and the rotary speed of the motor, ϕ, and four continuity equations associated with the pump pressure, P_s, the control pressure, P_y, the load pressure, P_L, and the load pressure sensed at the LS regulator, P_{Ls}.

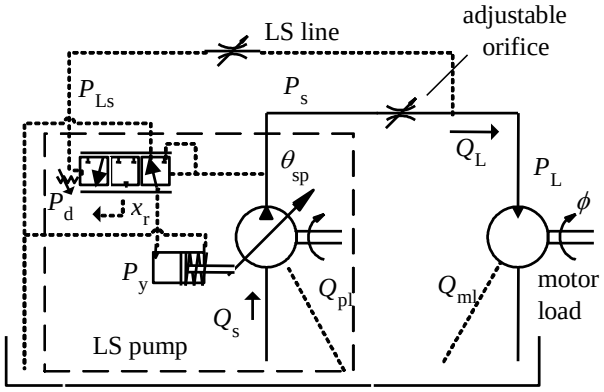

Fig. 1: *Schematic of the load sensing system*

2.1 Displacement of the LS Regulator Spool

Because the flow rates, Q_{r1} and Q_{r2}, through the LS regulator are very small, the steady state and transient flow forces can be neglected. The transfer function relating the regulator spool position to the $P_s - P_{Ls}$:

$$G_r(s) = \frac{X_r(s)}{P_s(s) - P_{Ls}(s)} = \frac{K_r}{\frac{s^2}{\omega_r^2} + \frac{2\zeta_r s}{\omega_r} + 1} \tag{1}$$

where $K_r = \frac{A_r}{k_r}$, $\omega_r = \sqrt{\frac{k_r}{m_r}}$ and $\zeta_r = \frac{B_r}{2\sqrt{m_r k_r}}$

2.2 Swash Plate Angle

Kavanagh et al (1987) developed a dynamic model that reflects the "back pressure" on the pump due to the pump pressure acting on the pistons. The transfer function based on the non-linear model is found to be:

$$\theta_{sp}(s) = G_{sp}(s)\left(K_{sps}P_s(s) - K_{spy}P_y(s)\right) \tag{2}$$

where

$$G_{G_{sp}}(s) = \frac{1}{\frac{s^2}{\omega_{sp}^2} + \frac{2\zeta_{sp}s}{\omega_{sp}} + 1}$$

$$\omega_{sp} = \sqrt{\frac{K_{sp} + K_{pr3}P_{s0}}{J_{sp}}}$$

$$\zeta_{sp} = \frac{B_{sp}}{2\sqrt{J_{sp}\left(K_{sp} + K_{pr3}P_{s0}\right)}}$$

$$K_{sps} = \frac{K_{pr2} - K_{pr3}\theta_{sp0}}{K_{sp} + K_{pr3}P_{s0}}$$

and $K_{spy} = \frac{R_{py}A_y}{K_{sp} + K_{pr3}P_{s0}}$

It is noted that ω_{sp}, ζ_{sp}, K_{sps} and K_{spy} ,depend on the steady state operating point, θ_{sp0} and P_{s0}.

2.3 Control Pressure in the Control Piston

The relationship between the control piston pressure P_y, the supply pressure P_s, regulator spool position x_r and the swash plate angle θ_{sp} is found to be (Wu, 2003):

$$P_y(s) = G_y(s)\left(K_{yr}X_r(s) + K_{ys}P_s(s) + K_{ysp}s\theta_{sp}(s)\right) \tag{3}$$

where:

$$G_y(s) = \frac{1}{\frac{s}{\omega_y} + 1}$$

$$\omega_y = K_{py} = \frac{\beta\left(K_{cr1} + K_{cr2}\right)}{V_{ymax} - A_y R_{py} \cdot \tan\left(\theta_{sp0}\right)}$$

$$K_{yr} = \frac{K_{qr1} + \left|K_{qr2}\right|}{K_{cr1} + K_{cr2}}$$

$$K_{ys} = \frac{K_{cr1}}{K_{cr1} + K_{cr2}}$$

$$K_{ysp} = \frac{R_{py}A_y}{\cos^2\theta_{sp0}\left(K_{cr1} + K_{cr2}\right)}$$

and (Wu, 2003)

$$K_{qr1} = \frac{\partial Q_{r1}}{\partial x_r} = \frac{C_d w_r\left(1 - (1+X)e^{-X}\right)}{(1-\varepsilon)\left(1 - e^{-X}\right)^2}\sqrt{\frac{2}{\rho}\left(P_{s0} - P_{y0}\right)}$$

$$\varepsilon = \frac{\left(-a\delta_1 e^{-\frac{\delta_1}{C_{d\infty}}\sqrt{\mathrm{Re}}} - b\delta_2 e^{-\frac{\delta_2}{C_{d\infty}}\sqrt{\mathrm{Re}}}\right)\sqrt{\mathrm{Re}}}{2C_d}$$

$$K_{qr2} = \frac{\partial Q_{r2}}{\partial x_r} = \frac{C_d w_r\left((1-X)e^{X} - 1\right)}{(1-\varepsilon)\left(e^{X} - 1\right)^2}\sqrt{\frac{2}{\rho}P_{y0}}$$

$$K_{cr1} = \frac{\partial Q_{r1}}{\partial \Delta P} = \frac{C_d w_r x_{r0}}{(1-\varepsilon)\left(1 - e^{-X}\right)\sqrt{2\rho\left(P_{s0} - P_{y0}\right)}}$$

$$K_{cr2} = \frac{\partial Q_{r2}}{\partial P_y} = \frac{C_d w_r x_{r0}}{(1-\varepsilon)\left(e^{X} - 1\right)\sqrt{2\rho P_{y0}}}$$

2.4 Pump Pressure

The transfer function relating the pump pressure P_s to the swash plate angle θ_{sp}, regulator spool position x_r, the control piston pressure P_y and the load flow Q_L is:

$$P_s(s) = G_s(s)\left(C_p\theta_{sp}(s) - K_{qr1}X_r(s) + K_{cr1}P_y(s) - Q_L(s)\right) \tag{4}$$

where

$$G_s(s) = \frac{K_s}{\frac{s}{\omega_s} + 1}$$

$$\omega_s = \frac{\beta\left(K_{cr1} + c_{pl}\right)}{V_p}$$

$$K_s = \frac{1}{K_{cr1} + c_{pl}}$$

and $C_p = \dfrac{NA_p R_p \omega}{\pi \cdot \cos^2\left(\theta_{sp0}\right)}$

The flow rate through the flow orifice, $Q_L(s)$, can be expressed by the standard linearized formula of the orifice equation (Merritt, 1967), since the load flow through the adjustable orifice is assumed turbulent.

$$Q_L(s) = K_q X(s) + K_c\left(P_s(s) - P_L(s)\right) \tag{5}$$

where

$$K_q = C_d w \sqrt{\frac{2}{\rho}\left(P_{s0} - P_{L0}\right)}$$

$$K_c = \frac{C_d w x}{\sqrt{2\rho\left(P_{s0} - P_{L0}\right)}}$$

2.5 Load Pressure and Rotary Speed of the Motor

The transfer functions relating the load pressure P_L to the load flow Q_L and the rotary speed of the load ϕ to the load flow Q_L are found to be:

$$H_L(s) = \frac{P_L(s)}{Q_L(s)} = \frac{K_L\left(\dfrac{s}{\omega_{L0}} + 1\right)}{\dfrac{s^2}{\omega_L^2} + \dfrac{2\zeta_L s}{\omega_L} + 1} \tag{6}$$

and

$$G_\varphi(s) = \frac{\phi(s)}{Q_L(s)} = \frac{K_\varphi}{\dfrac{s^2}{\omega_L^2} + \dfrac{2\zeta_L s}{\omega_L} + 1} \tag{7}$$

where

$$K_L = \frac{B_m}{c_{ml} B_m + D_m^2}$$

$$\omega_L = \sqrt{\frac{\beta\left(c_{ml} B_m + D_m^2\right)}{V_m J_m}}$$

$$\zeta_L = \frac{V_m B_m + c_{ml} J_m \beta}{2\sqrt{J_m V_m \beta\left(c_{ml} B_m + D_m^2\right)}}$$

$$\omega_{L0} = \frac{B_m}{J_m}$$

and

$$K_\varphi = \frac{1}{D_m + \dfrac{c_{ml} B_m}{D_m}}$$

2.6 Load Sensing Line

It is assumed that the movement of the LS spool at the LS regulator has a negligible effect on the sensed load pressure, P_{Ls}: thus the transfer function relating P_{Ls} to the load pressure P_L *is* given by

$$G_{Ls}(s) = \frac{P_{Ls}(s)}{P_L(s)} = \frac{1}{\dfrac{s}{\omega_{Ls}} + 1} \tag{8}$$

where

$$\omega_{Ls} = \frac{\beta}{V_{Ls} R_{Ls}}$$

It is now necessary to discuss the nonlinear models, linearization of the models and transfer functions of the components in the LS system. The linearized equations and transfer functions of these components are steady state operating point dependent involving θ_{sp0}, P_{s0}, x_{r0}, P_{y0}, θ_{sp0}, P_{s0} and P_{L0}. The transfer functions generated in this section are only valid at a particular steady state operating point if and only if the value of these variables exist at the operating point and are defined. The following section will discuss the steady state operating conditions, which make these transfer functions valid, and will demonstrate the procedure for the calculation of the operating point.

3 Steady State Operating Conditions

In order to determine if the operating point exists and to calculate the value of state variables at the operating point, the different operating regions must be considered to take into account the complete range of system operation. For example, when the LS pump is fully stroked, Eq. 2 does not apply and the operating point θ_{sp0} becomes θ_{spmax}. The pump becomes fully stroked because the spool of the critically lapped LS regulator in Fig. 1 moves to the right side. The control chamber (P_y) is exposed to tank (P_T) and, consequently, control pressure (P_y) becomes zero. Therefore, the different operating conditions of the LS system depend on the operation of the LS regulator.

The critically lapped spool design of the LS regulator requires special consideration when evaluating the operating point. For the LS system under steady state conditions, the time derivatives of the state variables are zero. It was shown by Wu that

$$Q_{r1} = \frac{C_d w_r x / d}{1 - e^{-x/d}} \sqrt{\frac{2}{\rho}\left(P_s - P_y\right)} \tag{9}$$

$$Q_{r2} = \frac{C_d w_r x / d}{e^{x/d} - 1} \sqrt{\frac{2}{\rho} P_y} \tag{10}$$

Under steady state the equation for Q_r in its functional form becomes

$$Q_{r1}\left(x_{r0}, P_{s0}, P_{y0}\right) = Q_{r2}\left(x_{r0}, P_{y0}\right) \tag{11}$$

Figure 2 shows three possible positions of the spool. For a critically lapped LS regulator, one of the orifices

or both are always lapped. If the leakage flow through either orifice under lapped status is neglected, Eq. 11 gives rise to the identities

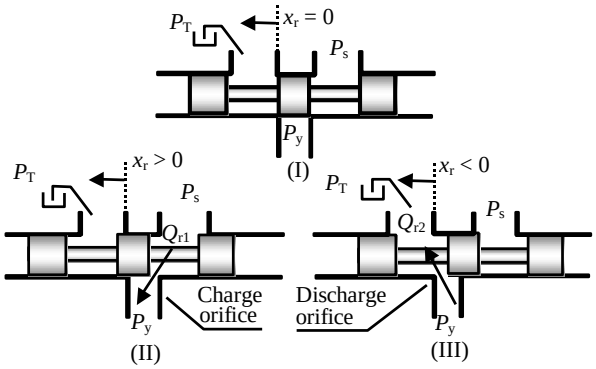

Fig. 2: *Three operating conditions of the LS spool (I) critically lapped (II) control chamber charged (III) control chamber discharged*

$$Q_{r1}\left(x_{r01}, P_{s01}, P_{y01}\right) = 0 \tag{12}$$

$$Q_{r2}\left(x_{r02}, P_{y02}\right) = 0 \tag{13}$$

where the subscript "$_{01}$" in Eq. 12 represents the operating point with $x_{r0} > 0$ (i.e. the "charge" orifice is open). The subscript "$_{02}$" in Eq. 13 represents the operating point with $x_{r0} < 0$ (i.e. the "discharge" orifice is open). Wu et al (2002(1)) described the operation of an LS system with a critically lapped LS regulator under three different conditions (Condition I, II and III).

For Condition I: $x_{r0} = 0$ ($Q_{r1} = 0$ and $Q_{r2} = 0$); this condition is obvious because the valve is critically lapped.

For Condition II: $x_{r0} > 0$ ($Q_{r1} = 0$); this only occurs if $P_{y0} = P_{s0}$.

For Condition III: $x_{r0} < 0$ ($Q_{r2} = 0$); this can only occur if $P_{y0} = 0$ and $P_T = 0$.

The three conditions describe "possible" scenarios of the LS regulator with a critically lapped spool under steady state conditions in which the flow rates are zero. Whether the operating point exists or is stable for each condition depends upon equations describing other parts of the LS system (i.e. the control piston, pressure control pump and the load in Fig. 1), and in particular, the steady state control characteristic of the pressure control pump. Figure 3, in which the control pressure, P_y, is plotted as a function of the pump pressure, P_s, and swash plate angle, θ_{sp} identifies the operating region where Condition II or III apply. The minimum swash plate angle, θ_{spmin}, is zero and the maximum, θ_{spmax}, is 0.32 radians for the pump studied.

Condition I cannot be shown in Fig. 3 as there is no explicit relationship between P_y and P_s for $x_r = 0$. Thus, P_{y0} and P_{s0} must be mathematically derived from other steady state equations. It is reasonable to expect that the solution may be any point in regions (A) and (B) which represent steady state operating regions permitted by the pressure control pump. However, any solution in region (A) does not make physical sense in the LS mode because P_y cannot be greater than P_s under steady state conditions. Therefore, only solutions in region (B) can be considered for $x_r = 0$.

Under the critically lapped condition, the pressure differential across the flow control valve is equal to, P_d, due to x_{r0} being zero. The load pressure, P_{L0}, the pump pressure, P_{s0}, the swash plate angle, θ_{sp0}, and the control pressure, P_{y0}, can be derived to be

$$P_{L0} = \frac{1}{\left(c_{ml} + \dfrac{D_m^2}{B_m}\right)}\left[C_d w x\sqrt{\frac{2P_d}{\rho}} + \frac{D_m T_{mf}}{B_m}\right] \tag{14}$$

$$P_{s0} = P_d + P_{L0} \tag{15}$$

$$\theta_{sp0} = \tan^{-1}\left[\frac{\pi}{NA_p R_p \omega}\left(C_d w x\sqrt{\frac{2P_d}{\rho}} + c_{pl} P_{s0}\right)\right] \tag{16}$$

$$P_{y0} = \frac{T_{sp}}{R_{py} A_y} + \frac{K_{pr2}}{R_{py} A_y} P_{s0} - \left(\frac{K_{sp}}{R_{py} A_y} + \frac{K_{pr3}}{R_{py} A_y} P_{s0}\right)\theta_{sp0} \tag{17}$$

Consider Condition II. This condition requires that the control pressure, P_y, be equal to the pump pressure, P_s (see Fig. 3). Possible operating points under Condition II must be on the line ($P_y = P_s$) and within θ_{spmin} and θ_{spmax}; this line is also the boundary between regions (A) and (B). Pressures P_s and P_y at two terminal points can be determined by

$$P_{s1} = \frac{T_{sp} - \theta_{spmax} K_{sp}}{\theta_{spmax} K_{pr3} + R_{py} A_y - K_{pr2}} \tag{18}$$

and

$$P_{s2} = \frac{T_{sp}}{R_{py} A_y - K_{pr2}} \tag{19}$$

The specific operating point under Condition II must also be mathematically determined by the following equation set

$$\frac{NA_p R_p \omega \tan\left(\theta_{sp}\right)}{\pi} = C_d w x\sqrt{\frac{2}{\rho}\left(P_s - P_L\right)} - c_{pl} P_s \tag{20}$$

$$\theta_{sp}\left(P_s\right) = \frac{T_{sp} + \left(K_{pr2} - R_{py} A_y\right) P_s}{K_{sp} + K_{pr3} P_s}$$

$$\left(0 \le \theta_{sp} \le \theta_{spmax} \quad \text{and} \quad P_y = P_s\right) \tag{21}$$

$$P_L = \frac{-b_2 + \sqrt{b_2^2 - 4b_1 b_3}}{2b_1} \tag{22}$$

where $b_1 = a_1^2$, $b_2 = a_3 - 2a_1 a_2$, and $b_3 = a_2^2 - a_3 P_s$. The coefficients, a_1, a_2, and a_3, can be further expressed as $a_1 = c_{ml} + \dfrac{D_m^2}{B_m}$, $a_2 = \dfrac{D_m T_{mf}}{B_m}$, and $a_3 = \dfrac{2C_d^2 w^2 x^2}{\rho}$.

Consider Condition III. This condition requires that the control pressure, P_y, be zero. However, Fig. 3 indicates that Condition III ($P_y = 0$) is outside the normal steady state operating region (B) of the pressure control pump. In fact, Condition III represents the "fully stroked" status of the pressure control pump where the swash plate angle is limited to the maximum value.

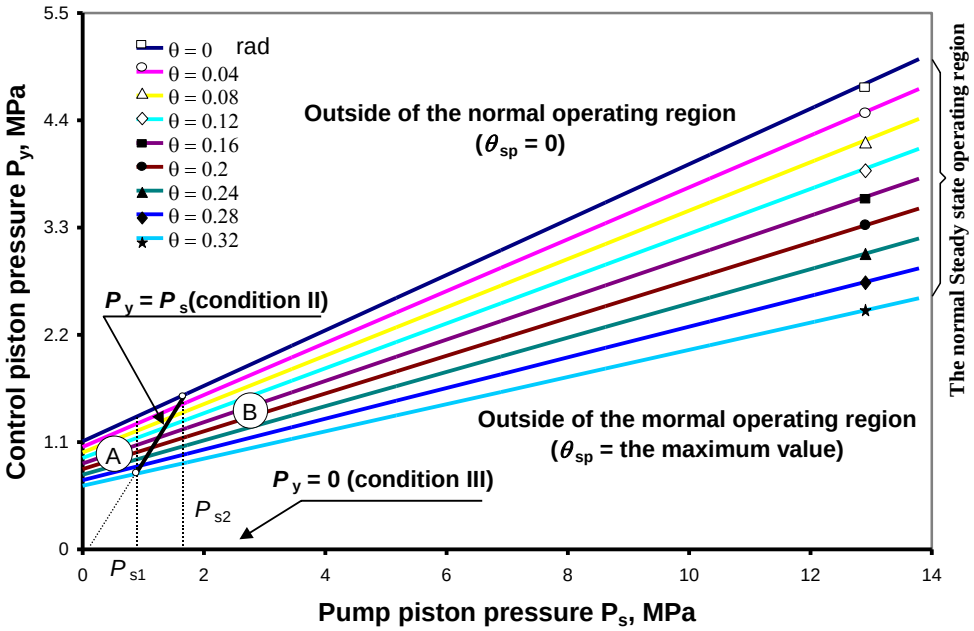

Fig. 3: *Steady state characteristics of the pressure control pump*

This often occurs if the pressure setting (such as P_d) of the LS system or the opening of the flow orifice (x_v) is very large, or the load is overrunning requiring more flow than the pump can deliver.

The load pressure and pump pressure under Condition III are determined by

$$P_{L0} = \frac{1}{\left(c_{ml} + \frac{D_m^2}{B_m}\right)}\left[\frac{NA_pR_p\omega\tan\theta_{spmax}}{\pi} + \frac{D_mT_{mf}}{B_m}\right] \quad (23)$$

$$P_{s0} = P_{L0} + \frac{\rho}{2}\left(\frac{NA_pR_p\omega\tan\theta_{spmax}}{\pi C_dA_v}\right)^2 \quad (24)$$

4 Procedure for Solving for the Steady State Operating Point

This section presents a flow chart of the steps involved to solve for the steady state operating point of the LS system (Fig. 4). An operating condition must first be assumed - for example - the normal operating Condition I (Step (1) in Fig. 4). Equations 14 through 17 give the steady state operating point directly (Step (2)). Then, Steps (3) and (4) determine if the result satisfies the essential conditions.

It is impossible in practice for the swash plate angle to be larger than the maximum value. If the calculation result gives this result, this indicates that the LS system cannot operate under Condition I. In this case, the LS system must operate under Condition III. Therefore, the steady state operating point should be calculated by Eq. 23 and 24. It is noted that the solutions under Conditions I and III do not require an iterative calculation.

If the control pressure, P_{y0}, computed by Eq. 17 in Step (2) is larger than the pump pressure, P_{s0}, then this situation results in a physically unrealizable steady state condition. In this case, the LS system must operate under Condition II. Equations 20 through 22 cannot give a direct expression of P_{s0}, P_{L0} and θ_{sp0} in the same way as Condition I and must be solved iteratively (thin line box in Fig. 4).

5 The LS System and the Experiment Setup

In order to validate these models, the experimental system shown in Fig. 5 was assembled. A load sensing pump and its regulator were connected to a controlled servo-valve. The supply to the servo valve was provided by a separate pressure source. The pump supplied flow to a hydraulic motor with a load that was artificially created and controlled by a relief valve in the return line of the motor. A sinusoidal signal to the servo valve provided the required frequency input to the system. Appropriate transducers were carefully calibrated before and after each test and provided the required information to the data acquisition system. Also included in the experimental setup were a signal generator, a tachometer, a signal analyzer, and an oscilloscope. All tests were conducted at a common fixed temperature (35 $\pm$ 3°C) and were repeated several times on separate days to ensure data repeatability. Details of the system are provided.

Since the equations were in transfer function form, and because the equations were operating point sensitive, frequency responses were chosen as the form to validate the equations. For comparative frequency response analysis, it was essential that the input signal (the opening of the adjustable orifice, x) be generated within a certain bandwidth. The valve chosen for this purpose was a two-stage servo valve (model: MOOG 72-102) with the pilot stage connected to an external hydraulic power supply. The relief valve (1) was used to create a backpressure on the motor load that was used

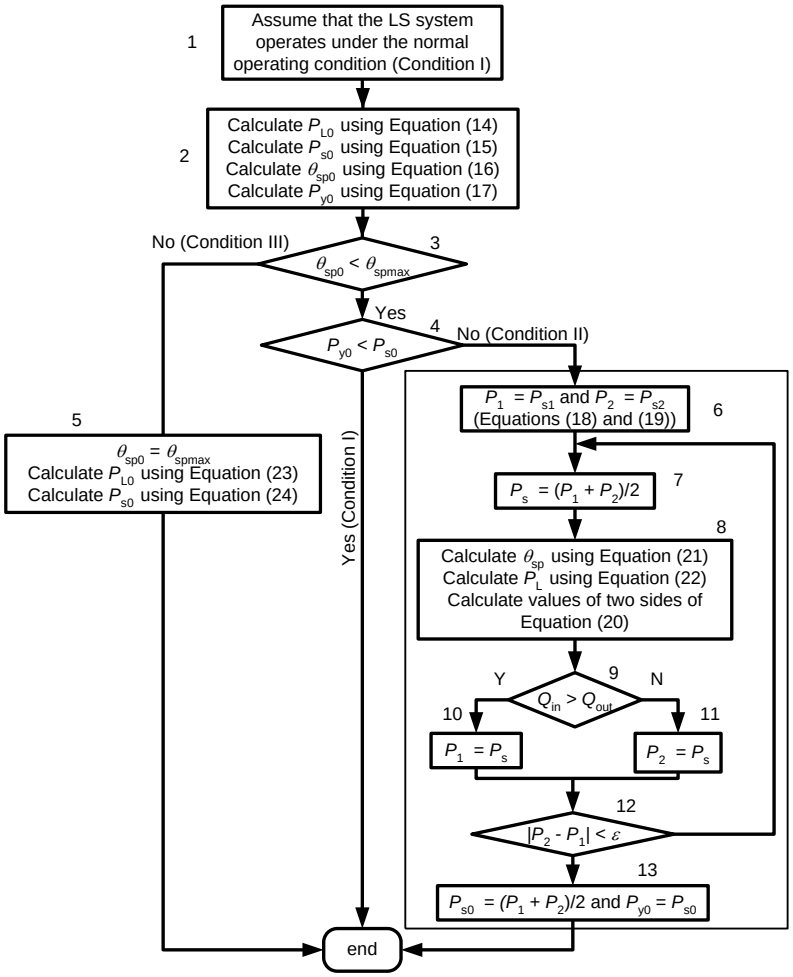

Fig. 4: *Flow chart of justifying steady state operating condition and calculating operating point*

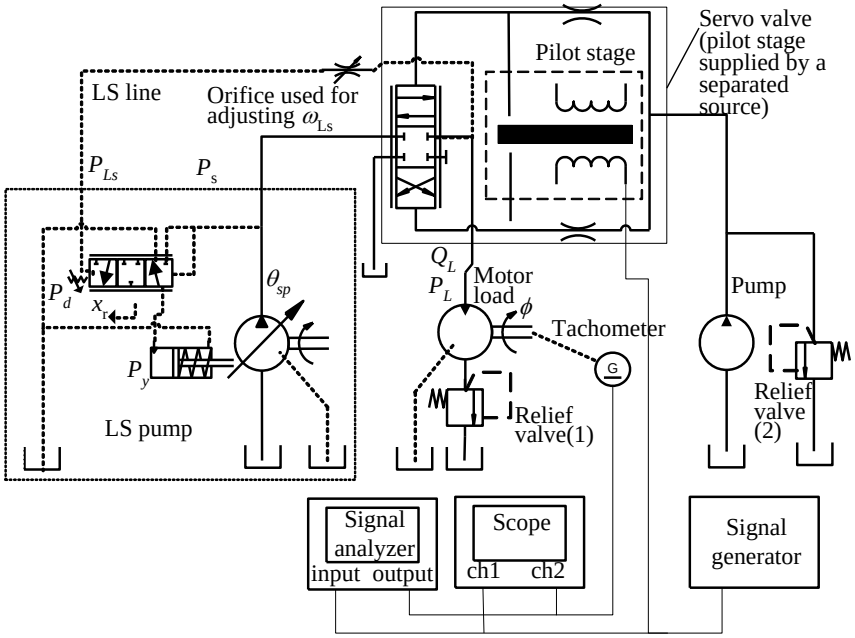

Fig. 5: *Experimental system to determine the frequency response of the LS system*

to adjust the operating point of the LS system. A tachometer (model: KEARFOTT CM-09608007) was used to measure the rotary speed of the motor load. Appropriate transducers for measuring the average values of the state variables, P_{s0}, P_{y0}, P_{L0}, x_{r0}, θ_{sp0} and Q_{L0}, at the chosen operating point were installed. The signal generator provided a dynamic input signal to control the servo valve orifice opening and a signal analyzer was employed to directly obtain the experimental Bode plot.

The parameters required for the model were obtained from the experimental system and are listed in Table 1 (Appendix A). All parameters with a "*" represent adjustable parameters. A_v is the cross sectional area which is proportional to the adjustable orifice opening, x, (Note: the orifice of the servo valve was rectangular). The pressure differential setting, P_d, the damped natural frequency in the LS line, ω_{Ls}, and the resistant torque of the load, T_{mf}, were adjustable. The bandwidth of the experimental system was limited (<20Hz) due to the finite bandwidth of the servo valve and the limited resolution of the tachometer.

6 Comparison of Model Predictions and Experimental Results

The transfer functions of the overall LS system relating motor rotary speed, $\phi(s)$, to the adjustable orifice opening, $X_v(s)$, were developed for the three operating conditions (Wu et al (2003)). It was found that the LS system model could be simplified into a 5th order dynamic model for Conditions I and II, and a 3rd order model for Condition III. Experimentally, motor rotary speed, ϕ, and adjustable orifice opening, x, were convenient variables to enable verification of the LS transfer functions at the different operating conditions.

6.1 Condition I ($x_{r0} = 0$, $P_{s0} - P_{L0} = P_d$)

For the experimental tests under Condition I, the operating point of the excitation signal to the servo valve was such that the flow rate, Q_L, was 13 l/min with the orifice area, A_v, estimated to be 11 mm^2. The adjustable parameters were set to the values shown in Table 2 (Appendix B) by adjusting the relief valve (1) to a cracking pressure of approximately 3.5 MPa. The linearized parameters, model parameters and the coefficients of the system transfer function (Wu, 2003) were determined as listed in Table 2. Finally, the poles of the transfer function that relate the motor rotary speed, $\phi(s)$, to the adjustable orifice opening, $X_v(s)$, were obtained.

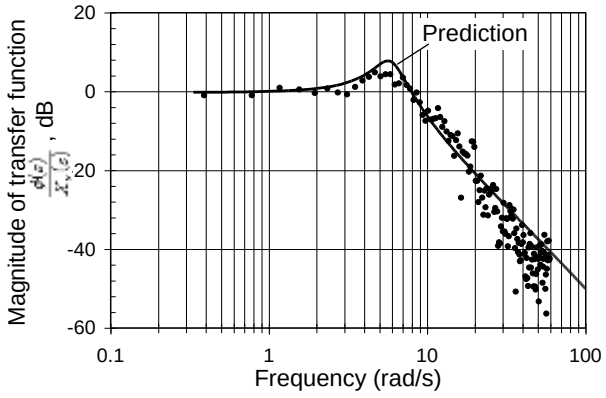

Fig. 6: *Comparison of magnitudes between the measured and predicted results*

Figures 6 and 7 show a comparison of Bode diagrams between the model (predicted, Wu et al (2003)) and the measured values. Figure 6 indicates that the model is a close representation of the actual system, particularly at lower frequencies. The phase shift prediction is somewhat off in the mid frequency range, but the crossover frequency prediction at 90° is very close. There is a resonance peak near 6 rad/s. This is a result of a pair of dominant conjugate poles ($s_{1,2}$ = -0.6 ±6j) which yield a small damping ratio (ζ = 0.1).

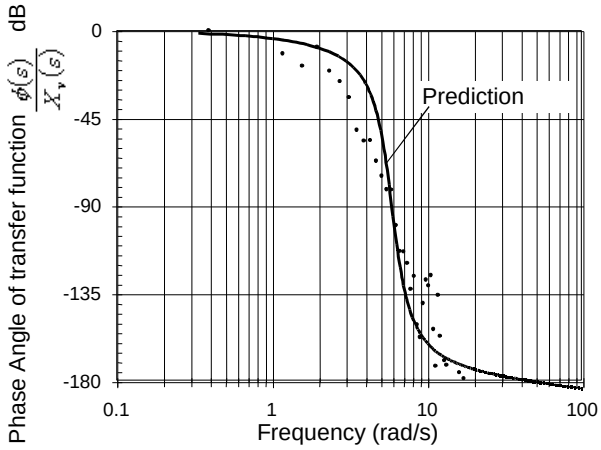

Fig. 7: *Comparison of the phase angles between the measured and predicted results*

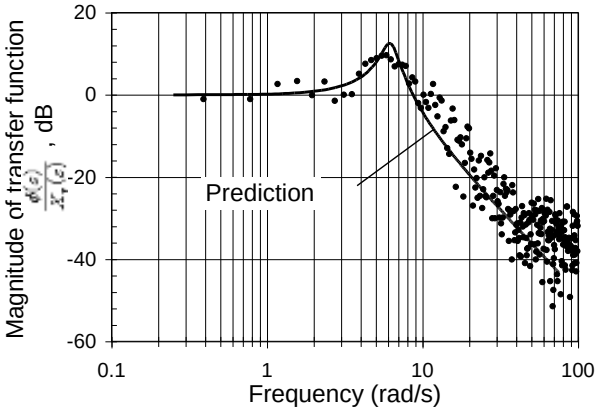

Fig. 8: *Comparison of magnitudes between the measured and predicted results with a small opening of the adjustable orifice*

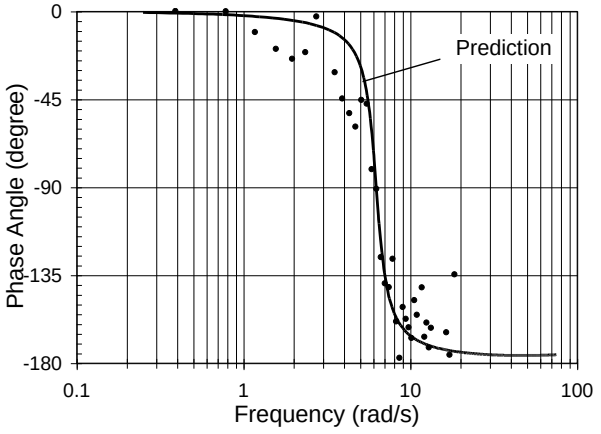

Fig. 9: *Comparison of the phase angles between the measured and predicted results with a small opening of the adjustable orifice*

For comparison, the frequency responses at a smaller orifice opening, x, were obtained. A comparison be-

tween the predicted and measured magnitudes and phases are shown in Fig. 8 and 9. A resonant peak exists near 7 rad/s. This is again a consequence of a pair of dominant conjugate poles ($s_{1,2}$ = -0.5 ± j7.3) with a small damping ratio (ζ = 0.07).

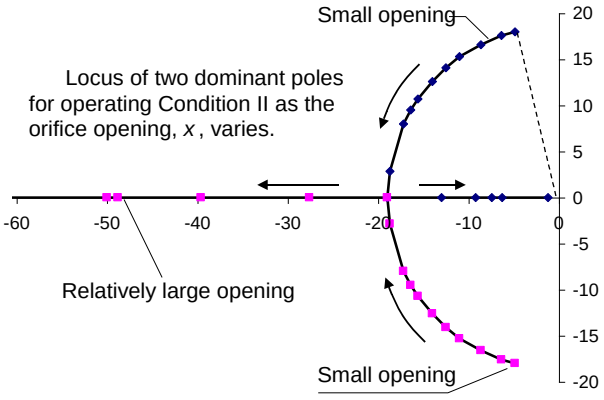

Fig. 10: *Root locus of the LS system for Condition II*

A comparison of Fig. 8 and 6 indicate that at the smaller orifice opening, *x*, a higher resonant peak in magnitude occurred. It can also be observed that the experimental plot of Fig. 8 has a larger scatter compared to Fig. 6. This is because the signal to noise ratio at the small opening is larger than that at the larger opening; this also has a large effect on the measurement of phase, as can be observed in Fig. 9. What is significant is that the model does predict a change in both the damped natural frequency and the damping ratio, which is consistent with the experimental results.

6.2 Condition II ($x_{r0} > 0$ and $P_{y0} = P_{s0}$)

Based on the model for operating Condition II, a pair of dominant poles exist which are sensitive to the operating point and subsequently are affected by the opening of the adjustable orifice, *x*. Figure 10 shows how the locus of the pair of dominant poles changes as the opening of the adjustable orifice changes. When the opening begins to increase (from zero), the dominant poles become a pair of complex conjugate poles. The corresponding undamped natural frequency is 18 rad/s and the damping ratio is very small (the smaller the opening, the smaller the damping ratio). When the opening increases to a specific value (corresponding to a low flow rate near 0.87 litre/min), the damping ratio becomes greater than 0.7. When the opening increases further, the damping ratio increases to 1. The model predicts that another pair of conjugate poles with positive real parts exist in the high frequency region, (about 100 ~ 300 rad/s, not shown in Fig. 10) when the opening, *x*, is large. However, this pair of poles is approximately cancelled by a pair of zeros near the same locations. Due to the high frequency of these poles (in the region of 100 ~ 300 rad/s), it is difficult to verify their presence experimentally.

In order to verify that the undamped natural frequency of 3 Hz (18 rad/s) exists in the experimental system as predicted by the model, the orifice opening, *x*, was set to a very small value (but not zero) and a Bode plot using a signal analyzer was attempted. As a consequence of the low signal-noise-ratio, reliable data could not be obtained to construct the Bode plot in the range of frequency desired. Therefore the following method was used to indicate where the undamped natural frequency occurred. When the pump operates, sufficient random noise is present in the system to excite a range of frequencies. Using spectral analysis of a signal from the system, an indication of the frequencies present in the system can be made.

Figure 11 shows the spectrum of the measured pump pressure, P_s. It is evident that several peaks exist in the trace. Some of the peaks can be attributed to the pump rotational speed and its harmonic frequencies as shown in Fig. 11. The peak at 3 Hz (18 rad/s) however, is attributed to the damped natural frequency of the LS system as predicted by the model. It was observed in other experiments that when the orifice opening was increased, the peak disappeared in the trace (damping ratio increases to 1). Therefore, it was concluded that the model did predict the main dynamic characteristic (the damped natural frequency) of the actual LS system. The actual damping ratio could only be indirectly deduced.

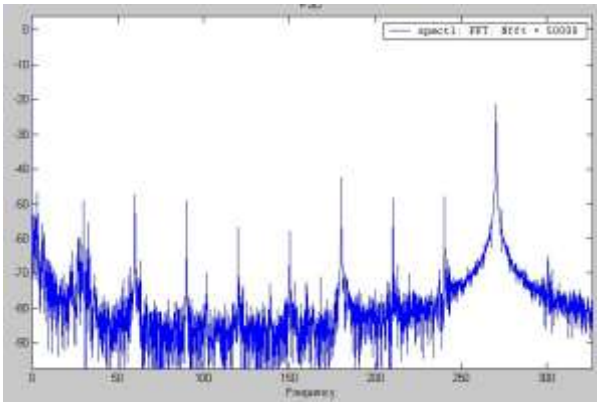

Fig. 11: *Power spectrum of the pump pressure at Condition II*

6.3 Condition III

When the LS system operates under Condition III, the LS pump acts as a fixed displacement pump since it is fully stroked. The circuit effectively becomes a simple fixed displacement pump/valve/motor configuration. The model for the experimental LS system, is given in the normalized form as

$$G(s) = \frac{0.000288(s+3)}{(s+30)(s^2+3.4s+38.54)} \qquad (25)$$

Equation 25 indicates that the system is stable because the transfer function has a zero (s_z = -3 rad/s), a pair of dominant conjugate poles ($s_{p1,2}$ = -1.7 ± j 6 rad/s), and an additional pole (s_{p3} = -30 rad/s). Figures 12 and 13 show a comparison of the predicted and experimental results in the form of Bode plots. It can be observed that the resonant frequency occurs near 6 rad/s (1 Hz). The comparison indicates that the experimental results have significant scatter at frequencies less than 2 rad/s. These results were repeatable but the actual reason for poor performance at low frequencies has not been adequately explained. This is being further explored. At higher frequencies, however, the predicted

results follow the trend of the experimental results quite closely and show very close correlation to the damped natural frequency and damping ratio.

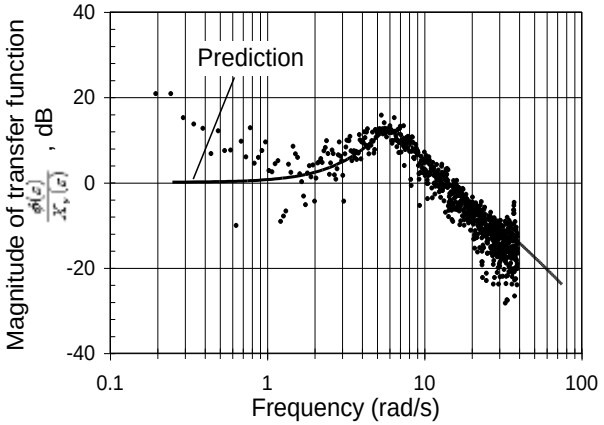

Fig. 12: *Comparison of the magnitude between the model and experimental results under Condition III*

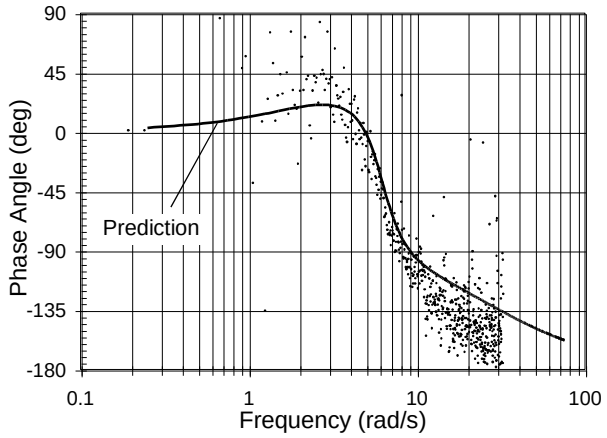

Fig. 13: *Comparison of the phase between the model and experimental results under Condition III*

7 Conclusions

In this paper, linearized models of an LS type system with a critically lapped regulator spool were introduced. Because the system operation strongly depends on the operating regions and the steady state operating point, steady state operating regions labeled as Conditions I, II and III have been defined. The procedure of justifying the operating condition and solving for the operating point was presented.

It was found that the LS system model could be simplified into a 5th order dynamic model for Conditions I and II, and a 3rd order model for Condition III. These models relate to the steady state operating point via the flow gain, K_q, the flow-pressure coefficient, K_c, and the non-linear dynamic equation of the pump swash plate.

The dynamic models of the LS system were validated experimentally under operating Conditions I, II and III. Bode plot comparisons (and in the case of Condition II, results from the frequency spectrum) indicated that the models were able to predict the dynamic performance of the LS system operating in Conditions I, II and III, with the exception of the lower frequency region of Condition III where scatter made it difficult to ascertain the results. It was concluded that the models could be used at different operating points with some confidence in predicting stability and transient performance.

Nomenclature

Δ	Differential of variables	[-]
"$_0$ "	Subscript which represents the operating point of a variable	[-]
A_p	Cross-sectional area of pump pistons	[m^2]
A_r	Cross-sectional area of the LS spool in the LS regulator	[m^2]
A_v	Orifice flow area	[m^2]
A_y	Cross-sectional area of the control piston of the pump	[m^2]
a, b	Coefficients in the empirical model C_d	[-]
a_i, b_i	Coefficients of s polynomial associated with transfer functions	[s^{-1}],[s^{-2}]
B_m	Damping coefficient of the motor	[Nms]
B_r	Damping coefficient of the LS spool	[Nm^{-1}s]
B_{sp}	Simplified constant (damping coefficient) of the control piston and swash plate assembly	[Nms]
C_d	Orifice discharge coefficient	[-]
$C_{d\infty}$	Fully turbulent flow / Orifice discharge coefficient	[-]
c_{ml}	Leakage coefficient of the motor	[m^{3}s^{-1}Pa^{-1}]
C_p	Dynamic gain of the LS pump	[m^{3}s^{-1}rad^{-1}]
c_{pl}	Leakage coefficient of the pump	[m^{3}s^{-1}Pa^{-1}]
D_m	Volumetric displacement of the motor	[m^3]
d	Equivalent height of square type orifice at the null position	[m]
G_{Ls}	Transfer function of the LS line	[-]
G_r	Transfer function of the LS spool displacement	[m·Pa^{-1}]
G_s	Transfer function associated with the pump volume	[Pa·s·m^{-3}]
G_{sp}	Transfer function associated with the swashplate of the LS pump	[-]
G_y	Transfer function associated with the control piston volume	[-]
G_ϕ	Transfer function associated with the motor speed	[rad·m^{-3}]
H_L	Transfer function of the load: $P_L(s)/Q_L(s)$	[Pa·m^{-3}s]
J_m	Moment of inertia of the motor and load.	[Nms^2]
J_{sp}	Average total moment of inertia of swash plate, yoke and piston assembly	[Nms^2]
K_c	Flow-pressure coefficient	[m^{5}s^{-1}N^{-1}]
K_{cr1}	Flow-pressure coefficient for the "charge" orifice of the LS regulator	[m^{5}s^{-1}N^{-1}]
K_{cr2}	Flow-pressure coefficient for the "discharge" orifice of the LS regulator	[m^{5}s^{-1}N^{-1}]

$K_{d\square}$	Linearization coefficient	[Pa·rad^{-1}]
K_L	Gain coefficient of the load transfer function	[Pa·m^{-3}s]
K_{pr2}	Pressure torque constant	[m^3]
K_{pr3}	Pressure torque constant	[m^{3}rad^{-1}]
K_{ps}	Linearization coefficient	[s^{-1}]
K_{py}	Linearization coefficient	[s^{-1}]
K_q	Flow gain of orifices	[m^{2}s^{-1}]
K_{qr1}	Flow gain for the "charge" orifice	[m^{2}s^{-1}]
K_{qr2}	Flow gain for the "discharge" orifice	[m^{2}s^{-1}]
K_r	Gain coefficient of the LS spool transfer function	[m·Pa^{-1}]
K_{xr}	Linearization coefficient	[Pa·m^{-1}s^{-1}]
K_s	Gain coefficient of the pump volume transfer function	[Pa·s·m^{-3}]
K_{sp}	Angular effective spring coefficient	[Nm·rad^{-1}]
K_{sps}	Gain coefficient of the swash plate transfer function with respect to the pump pressure	[rad·Pa^{-1}]
K_{spy}	Gain coefficient of the swash plate transfer function with respect to the control pressure	[rad·Pa^{-1}]
K_{yr}	Gain coefficient of the transfer function associated with the control volume to the LS spool displacement	[Pa·m^{-1}]
K_{ys}	Gain coefficient of the transfer function associated with the control volume to the pump pressure	[-]
K_{ysp}	Gain coefficient of the transfer function associated with the control volume to the swash plate angle	[Pa·s^{2}rad^{-1}]
K_ϕ	Gain coefficient of the load rotary speed transfer function	[rad·m^{-3}]
k_r	Spring coefficient of balance spring of the LS spool	[Nm^{-1}]
m_r	Mass of the LS spool	[kg]
N	The number of the pump pistons	[-]
P_d	Pressure differential setting across a simple orifice in the LS system or across a PC valve in the LSPC system	[Pa]
P_L	Load pressure	[Pa]
P_{Ls}	Load pressure at the end of LS line	[Pa]
P_s	Pump pressure	[Pa]
P_T	Tank pressure	[Pa]
P_y	Control piston pressure of the pressure control pump	[Pa]
Q	Flow rate	[m^{3}s^{-1}]
Q_L	Load flow rate	[m^{3}s^{-1}]
Q_{ml}	Leakage flow rate of the motor	[m^{3}s^{-1}]
Q_{pl}	Leakage flow rate of the pump	[m^{3}s^{-1}]
Q_{r1}	Flow rate through the "charge" orifice	[m^{3}s^{-1}]
Q_{r2}	Flow rate through the "discharge" orifice	[m^{3}s^{-1}]
Re	Reynolds number on an orifice	[-]
R_{Ls}	Flow resistance on the LS damping orifice	[m^{3}s^{-1}Pa^{-1}]
R_p	Moment arm of the pump piston	[m]
R_{py}	Moment arm of the control piston about pump shaft	[m]
T_{mf}	Resistant torque of the motor load	[Nm]
T_{sp}	Angular effective spring pretension	[Nm]
V_{Ls}	Volume in the LS line	[m^3]
V_m	Volume in the chamber between the flow valve (a simple orifice or a PC valve) and the motor	[m^3]
V_p	Volume of the pump chamber	[m^3]
V_y	Volume of the control piston chamber of pump	[m^3]
V_{ymax}	Maximum volume of the control piston chamber of pump	[m^3]
w	Rectangular orifice width	[m]
w_r	Width of the rectangular orifice for the control piston	[m]
x	Orifice flow opening	[m]
X	Dimensionless orifice opening	[-]
x_r	The displacement of the LS spool in the LS regulator	[m]
β	Bulk module of the fluid	[Nm^{-2}]
δ	Laminar flow coefficient of orifices	[-]
δ_1, δ_2	Attenuation coefficient in empirical model of C_d	[-]
ε	Modification coefficient of discharge coefficient, or Reynolds number	[-]
ϕ	Rotary speed of the motor	[rad·s^{-1}]
ρ	Fluid density	[kgm^{-3}]
θ_{sp}	Swash plate angle of the pump	[rad]
ω	Rotary speed of pump shaft	[rad·s^{-1}]
ω_L	Undamped natural frequency of the motor load	[s^{-1}]
ω_{L0}	Zero of the motor load transfer function	[s^{-1}]
ω_{Ls}	Damping break frequency of the LS line	[s^{-1}]
ω_{p0}	Zero of the LS pump transfer function	[s^{-1}]
ω_r	Undamped natural frequency of the LS spool	[s^{-1}]
ω_s	Break frequency of the pump volume associated with capacitance	[s^{-1}]
ω_{sp}	Undamped natural frequency of the swash plate	[s^{-1}]
ω_y	Break frequency of the control chamber	[s^{-1}]
ω_{ysp}	Equivalent break frequency	[s^{-1}]
ζ	Damping ratio	[-]

References

Bitner, D. and Burton, R. T. 1984(1). Experimental Measurement of Load Sensing Pump Parameters. *Proceeding of the 40th National Conference on Fluid Powe*r, Chicago, pp. 153-161.

Bitner, D. and Burton, R. T. 1984(2). Small Signal Model of a Load Sensing Pump. *Proceeding of the 40th National Conference on Fluid Power*, Chicago, pp. 107-112.

Bitner, D. 1986. *Analytical and Experimental Analysis of a Load Sensing Pump*. M. Sc. thesis, University of Saskatchewan, Canada.

Book, R. and Goering, C. E. 1997. Load Sensing Hydraulic System Simulation. *Applied Engineering in Agriculture*. ASAE Vol.13 (1), pp.17-25.

Erkkila, M. 1999. Practical Modelling of Load-Sensing Systems. *Proceeding of the Sixth Scandinavian International Conference on Fluid Power, SICFP'99*, Tampere, Finland, pp. 445.

Kappl, T.J. 2001. Semiempirical Model for Variable Displacement Pump with Load Sensing Regulator and Power Restrictor. *Proceedings of 2001 ASME International Mechanical Engineering Congress and Exposition*. New York, NY, USA. Nov. 11.

Kavanagh, G. P., Schoenau, G.J. and Burton, R.T. 1990. Dynamic Analysis of a Variable Displacement Pump. *ASME Journal of Dynamic Systems Measurement and Control*, Vol.112, No.1, pp.122.

Kim, S. D. and Cho, H. S. 1988. Stability Analysis of a Load-Sensing Hydraulic System. *Proceedings of the Institute of Mechanical Engineering*. Part A. Vol. 202, pp. 79-88.

Krus, P. 1988. On Load Sensing Fluid Power Systems. *Dissertation No.198*. Linkoping University, Sweden.

Lantto, B., Palmberg, J.O. and Krus, P. 1990. Static and Dynamic Performance of Mobile Load-sensing Systems with Two Different Types of Pressure-Compensated Valves. *SAE Technical Paper Series*. *SAE*. Sept. 10-13, pp. 251.

Lantto, B., Krus, P. and Palmberg, J.O. 1991. Interaction between Loads in Load-sensing Systems. *Proceeding of the 2nd Tampere International Conference on Fluid Power*. Linkoping, Sweden, pp. 53.

Merritt, H.E. 1967. *Hydraulic Control Systems.* John Wiley & Sons, Inc.

Palmberg, J. O., Krus, P. and Ding, K. 1985. Dynamic Response Characteristics of Pressure-Control Pumps. *The First International Conference on Fluid Power Transmission and Control*. Zhejiang University, Hangzhou, China, pp. 110.

Sakurai, Y. and Takahashi, K. 1997. Modelling and Simulation of a Load Sensing System by Bond-Graph Method. *Proceedings of the Fifth Scandinavian International Conference on Fluid Power*. Linkoping University. Vol. 3, pp.187-198.

Wu, D. 2003. Modeling and Experimental Evaluation of a Load -Sensing and Pressure Compensated Hydraulic System, PhD Thesis, University of Saskatchewan.

Wu, D., Burton, R., Schoenau, G. and Bitner, D. 2002(1). Establishing Operating Points for a Linearized Model of a Load Sensing System. *International Journal of Fluid Power*. Vol. 3, No. 2, pp. 47-54.

Wu, D., Burton, R., and Schoenau, G. 2002(2). An Empirical Discharge Coefficient Model for Orifice Flow. *International Journal of Fluid Power*. Vol. 3, No. 3.

Wu, D., Burton, R., Schoenau, G. and Bitner, D. 2003. Modeling of Orifice Flow Rate at Very Small Openings. *International Journal of Fluid Power*. Vol. 4, No. 1.

Zarotti, L. G. and Nervegna, N. 1988. Saturation Problems in Load Sensing Architectures. *Proceeding of the 43rd National Conference on Fluid Power, NCFP*, Chicago, pp. 393.

Acknowledgements

The authors acknowledge the financial support of NSERC Discovery Grants and the University of Saskatchewan scholarships.

Duqiang Wu
Received his M.Sc from Nanjing University of Science and Technology in China, 1984 and his PhD from the University of Saskatchewan in 2003. He was an Engineer (1986) at Shaanxi Mechanical and Electrical Institute in China, and a Visiting Scholar (1997) at University of Illinois at Urbana-Champaign. He is now a research engineer with Eaton Corp, Minneapolis.

Richard Burton
P.Eng, Ph.D, FASME, Burton is a Professor of Mechanical Engineering, University of Saskatchewan He is involved in research pertaining to the application of intelligent theories to control and monitoring of hydraulics systems, component design, and system analysis. He is a Fellow of ASME, a member of the executive of ASME, FPST Division, a member of the hydraulics' advisory board of SAE and NCFP and a convenor for FPNI.

Greg Schoenau
Professor of Mechanical Engineering at the University of Saskatchewan. He was head of that Department from 1993 to 1999. He obtained B.Sc. and M. Sc. Degrees from the University of Saskatchewan in mechanical engineering in 1967 and 1969, respectively. In 1974 he obtained his Ph.D. from the University of New Hampshire in fluid power control systems. He continues to be active in research in this area and in the thermal systems area as well. He has also held positions in numerous outside engineering and technical organizations.

Doug Bitner
MSc. Departmental Assistant Mechanical Engineering, University of Saskatchewan. Manager Fluid Power Laboratory and Control Systems Laboratory University of Saskatchewan.

Appendix A

Table 1: Parameters for the stability analysis of the LS system

Components	Parameter definition	Symbol	Value	Unit
Fluid properties	Bulk modulus	β	$1.38\text{x}10^{9}$	Nm^{-2}
	Fluid density	ρ	898	kgm^{-3}
	Fluid absolute viscosity at 25°C	μ	$1.74\text{x}10^{-4}$	m^2s^{-1}
LS regulator	Pressure differential of the adjustable orifice	P_d *	0.3 ~ 2.5	MPa
	LS spool cross-sectional area	A_r	$3.2\text{x}10^{-5}$	m^2
	LS spool balance spring constant	k_r	$6.1\text{x}10^{4}$	Nm^{-1}
	LS spool mass	m_r	$1.6\text{x}10^{-2}$	kg
	LS spool damping coefficient	B_r	2.21	Nsm^{-1}
	Equivalent opening of two orifices at null point	d_r	$2.5\text{x}10^{-5}$	m
	Equivalent width of two orifices at null point	w_r	$4\text{x}10^{-3}$	m
Control piston	Moment arm of the control piston about the shaft	R_{pv}	$5.5\text{x}10^{-2}$	m
	Cross-sectional area of the control piston	A_v	$3.36\text{x}10^{-4}$	m^2
	Minimum volume of the control piston chamber	V_{vmin}	$1.38\text{x}10^{-6}$	m^3
Pressure pump	Moment arm of the pump pistons about the shaft	R_p	$3.48\text{x}10^{-2}$	m
	Cross-sectional area of pump pistons	A_p	$2.07\text{x}10^{-4}$	m^2
	Pump outlet volume including the hose volume	V_p	$2.0\text{x}10^{-4}$	m^3
	Pump leakage coefficient	c_{pl}	$2.0\text{x}10^{-12}$	$\text{m}^5\text{s}^{-1}\text{N}^{-1}$
	Pump shaft speed	ω	183.5	rad-s^{-1}
	Angle coefficient of swash plate spring	K_{sp}	$1.42\text{x}10^{6}$	$\text{N-m}^{-2}\text{rad}^{-1}$
	Angle precompression of swash plate spring	T_{sp}	$1.11\text{x}10^{6}$	N-m^{-2}
	Pressure torque constant	K_{pr2}	$2.84\text{x}10^{-1}$	
	Pressure torque constant	K_{pr3}	$4.53\text{x}10^{-1}$	rad^{-1}
	Damping coefficient of the swash plate	B_{sp}	$5.5\text{x}10^{-1}$	Nsm
	Inertia of the swash plate	J_{sp}	$1.32\text{x}10^{-3}$	kgm^2
	Maximum swash plate angle	θ_{spmax}	$3.14\text{x}10^{-1}$	rad
Adjustable orifice	Discharge coefficient	C_d	0.63	
	Cross sectional area of the flow control orifice	A_v *	Variable	m^2
Motor and load	Damping coefficient of the motor and the load	B_m	0.056	Nms
	Motor inlet volume including the hose volume	V_m	$1.4\text{x}10^{-4}$	m^3
	Inertia of the motor and the load	J_m	$1.62\text{x}10^{-1}$	kgm^2
	Resistant torque of the load on the motor axis	T_{mf} *	0.2 ~	Nm
	Motor leakage coefficient	c_{ml}	$2.0\text{x}10^{-13}$	$\text{m}^5\text{s}^{-1}\text{N}^{-1}$
	Volumetric displacement of the motor	D_m	$2.57\text{x}10^{-6}$	$\text{m}^3\text{rad}^{-1}$
LS line	Damping frequency of the LS line	ω_{ls} *	0 ~ 500	rad-s^{-1}

Appendix B

Table 2: An example of determining parameters for the stability analysis

Adjustable parameters	A_v			Settable parameters	P_d	T_{mf}	ω_{Ls}
	11 mm^2				0.3 MPa	13.7 Nm	450 s^{-1}
Operating point	P_{s0}	P_{y0}	P_{L0}	x_{r0}	θ_{sp0}	Q_{L0}	ϕ_0
	7.6 MPa	3 MPa	7.3 MPa	-0.006 mm	0.055 rad	13 l/min	53 rad/s
Linearized parameters	K_{q1}	K_{q2}	K_{cr1}	K_{cr2}	K_c		
	0.099 m^2s^{-1}	-0.092 m^2s^{-1}	$0.5x10^{-12}$ $m^5s^{-1}N^{-1}$	0.8x10-12 $m^5s^{-1}N^{-1}$	$3.6x10^{-12}$ $m^5s^{-1}N^{-1}$		
Model parameters	K_p	K_s	K_L	ω_s	ω_L	ω_{sp}	ω_r
	$2x10^{-8}$ $m^5s^{-1}N^{-1}$	$5x10^{11}$ m ^{5}sN	$9.8x10^9$ $m^{-5}sN$	13.8 s^{-1}	18.6 s^{-1}	130 s^{-1}	1954 s^{-1}
	ω_y	ω_{L0}	ω_{p0}	ζ_r	ζ_L	ζ_{sp}	
	290 s^{-1}	0.34 s^{-1}	405 s^{-1}	0.0353	0.06	0.4	
Coefficients of TF	numerator			b_3	b_2	b_1	b_0
				$4.69x10^{-4}$	0.384	143	$2.95x10^4$
	Denominator	a_5	a_4	a_3	a_2	a_1	a_0
		$1.36x10^{-6}$	$0.94x10^{-2}$	5.96	803	1127	$2.95x10^4$
Poles of TF	s_1	s_2	s_3	s_4	s_5		
	-0.6+j6	-0.6-j6	-188	-499	-6248		